ELSEVIER

Journal of Power Sources 112 (2002) 8–12

JOURNAL OF POWER SOURCES

www.elsevier.com/locate/jpowsour

Lithium storage properties of nanocrystalline Ni_3Sn_4 alloys prepared by mechanical alloying

Heon-Young Lee[a], Serk-Won Jang[a], Sung-Man Lee[a,*], Seung-Joo Lee[b], Hong-Koo Baik[b]

[a]*Department of Advanced Material Science and Engineering, Kangwon National University, Chuncheon, Kangwon-do 200 701, South Korea*

[b]*Department of Metallurgical Engineering, Yonsei University, Seoul 120 749, South Korea*

Received 4 November 2001; accepted 18 January 2002

Abstract

Nanocrystalline Ni_3Sn_4 alloy powders prepared by high energy ball milling are examined as an anode for lithium-ion batteries. Ex situ X-ray diffraction (XRD) and differential capacity plots show that crystalline Ni_3Sn_4 has a low affinity for lithium. In the case of well-developed nanocrystalline Ni_3Sn_4, the lithium atoms reversibly react with tin atoms in the grain boundaries with no capacity fading for extended cycling.

Keywords: Ni_3Sn_4; Ball milling; Nanocrystalline; Grain boundary; Lithium-ion battery; Capacity

1. Introduction

Lithium alloys have been extensively studied as anodes for rechargeable lithium batteries as they show large capacity compared with the carbonaceous materials [1–3]. The main problem concerned with the use of these alloys is a substantial change in volume during charge–discharge cycling. This causes fast mechanical disintegration of the electrode and consequent very short cycle-life. The cycling performance of lithium alloys can be significantly improved if intermetallic and/or composite hosts are employed instead of pure metals. Several materials with enhanced performance have been proposed, such as $SnFe_2$ [4], $SnFe_2C$ [5], and Sn_5Cu_6 [6,7]. The mechanism for reversible lithium insertion and extraction in SnM alloys has been described as a displacement reaction in which Sn forms a lithium alloy Li_xSn and a nanosize inactive M matrix is created simultaneously. The latter may buffer the volume expansion of the active phase Sn, due to alloying with Li. Nevertheless, the capacity retention is still not as good as expected. The observed capacity fade has been attributed to [4] the agglomeration of the active phase Sn into larger grains.

On the other hand, a different mechanism for lithium insertion into nanostructured $SnMn_3C$ has recently been advanced, in which lithium atoms enter the nanostructured particles to react reversibly with tin atoms in the grain boundaries [8]. The cycle-life of this material was excellent. We have discovered that the intermetallic material, Ni_3Sn_4, behaves similarly.

This paper describes the synthesis of nanocrystalline Ni_3Sn_4 alloy powders. The electrochemical performance of these powders as electrodes in lithium cells is evaluated and the mechanism for lithium insertion is investigated by ex situ X-ray diffraction (XRD).

2. Experimental

Ni_3Sn_4 alloy powders were prepared using a commercial SPEX-8000 high energy ball mill with stainless-steel balls and vials. The charging of the elemental powders of nickel and tin as well as the milling were performed in an argon-filled glove box. The ball-to-powder weight ratio was 6:1. Milling was stopped every 10 min, at which time the assembly was allowed to cool. At regular intervals, a small amount of powder was taken for analysis by XRD and scanning electron microscopy (SEM).

Electrodes containing 75 wt.% sample, 15 wt.% carbon black, and 10 wt.% poly vinylidene fluoride (PVDF) were

* Corresponding author.
E-mail address: smlee@kangwon.ac.kr (S.-M. Lee).

0378-7753/02/$ – see front matter
PII: S0378-7753(02)00047-2

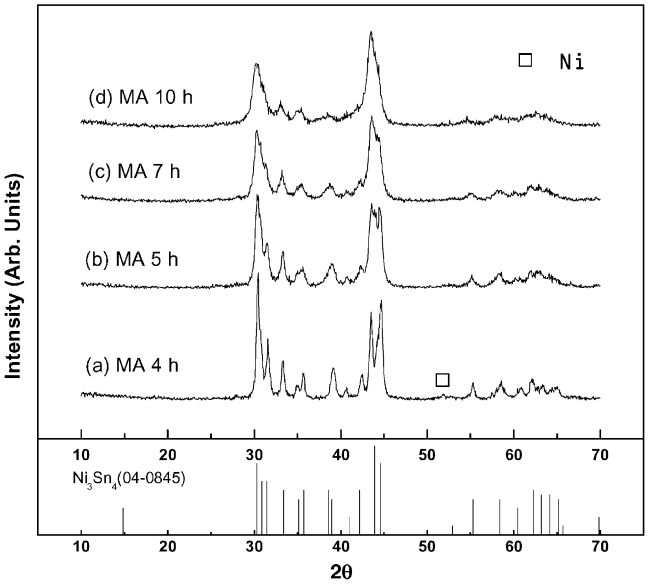

Fig. 1. XRD patterns at different times during ball milling of $Ni_{43}Sn_{57}$ powder.

coated on a thin copper grid. The coatings were dried in vacuum at 120 °C for 12 h. Cells for electrochemical characterization comprised a lithium metal electrode, a separator and a Ni_3Sn_4 electrode. The electrolyte solution, provided by Cheil industries Inc., Korea, was 1 M $LiPF_6$ in a ethylene carbonate/diethyl carbonate (EC:DEC = 1:1, v/v) mixed solvent. Cells were prepared in an argon-filled glove box and used 2016 coin-cell hardware. The cells were cycled galvanostatically at 0.2 mA cm^{-2} between 0 and 1.2 V. The cell temperature was maintained at 30 °C.

3. Results and discussion

The XRD patterns for the $Ni_{43}Sn_{57}$ powder mixture at different milling times are given in Fig. 1. After milling for 4 h, the peaks for pure nickel and tin almost disappear and peaks for crystalline Ni_3Sn_4 are detected. As the ball-milling time is increased, the diffraction peaks broaden. This indicates a reduction in crystallite size and incorporation of inhomogeneous strain in the crystallites.

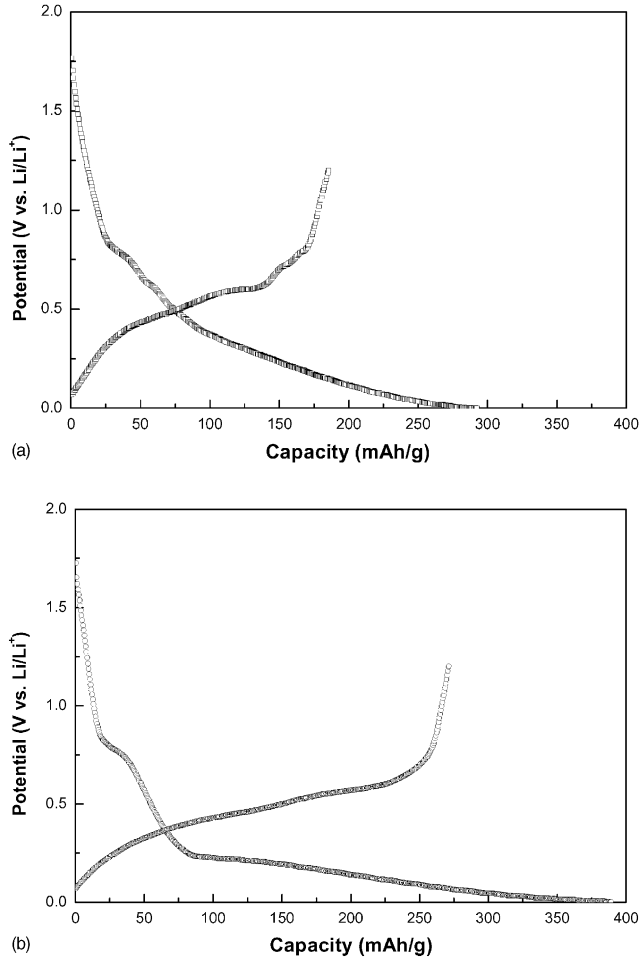

Fig. 2. First charge–discharge curves for material mechanically alloyed for (a) 4 h and (b) 10 h.

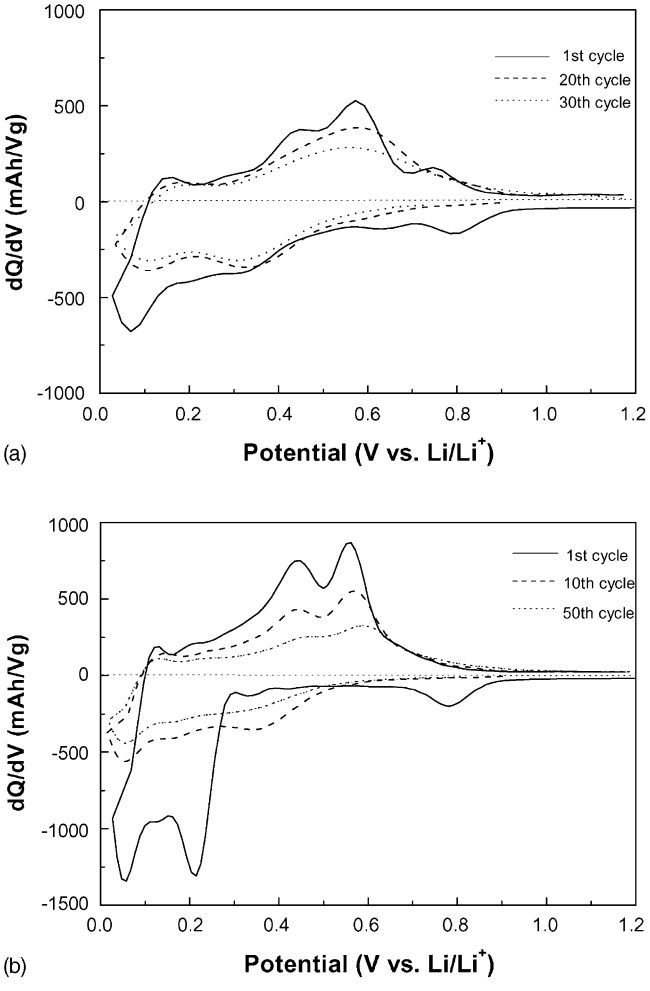

Fig. 3. Differential capacity vs. voltage for samples mechanically alloyed for (a) 4 h and (b) 10 h.

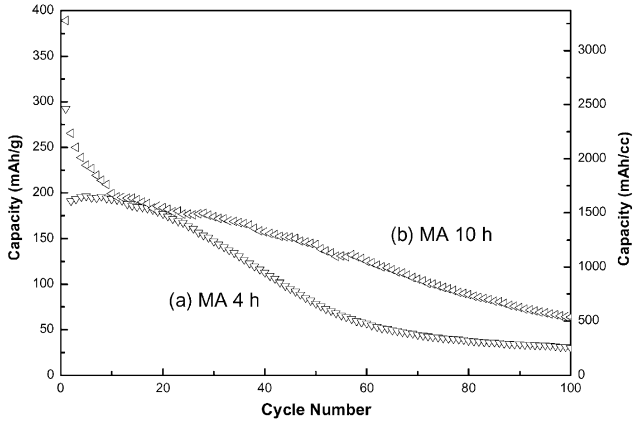

Fig. 4. Discharge capacity vs. cycle number for samples mechanically alloyed for 4 and 10 h.

The first charge and discharge curves of samples milled for 4 and 10 h are shown in Fig. 2(a) and (b), respectively. Lithium insertion into and extraction from Ni_3Sn_4 alloy are defined as discharge and charge, respectively. The two electrodes demonstrate markedly different behavior for charge–discharge profiles and capacities. The voltage profile of the sample milled for 4 h shows more prominent multistep reactions, which range from 0.0 to 0.8 V than that of the sample milled for l0 h.

The differential capacity versus voltage relationships for the same two materials are given in Fig. 3. On the first cycle, the differential-capacity curve is similar to that for pure tin [9] although the peaks are broader. This broad feature indicates that tin atoms are active but not aggregating into large regions [8]. As cycling proceeds, the differential-capacity curves change continuously, as shown in Fig. 3, which suggests that the microstructures of the two materials change and causes capacity fading. Plots of discharge capacity versus cycle number for the two electrodes are presented in Fig. 4. In order to investigate the reaction mechanism, ex situ XRD analysis was performed. The ex situ XRD patterns after the first discharge and charge to a given voltage are shown in Fig. 5(a) and (b). The pattern after 100 cycles is also shown. For the alloy milled for 4 h, the crystallinity of the Ni_3Sn_4 phase is maintained without

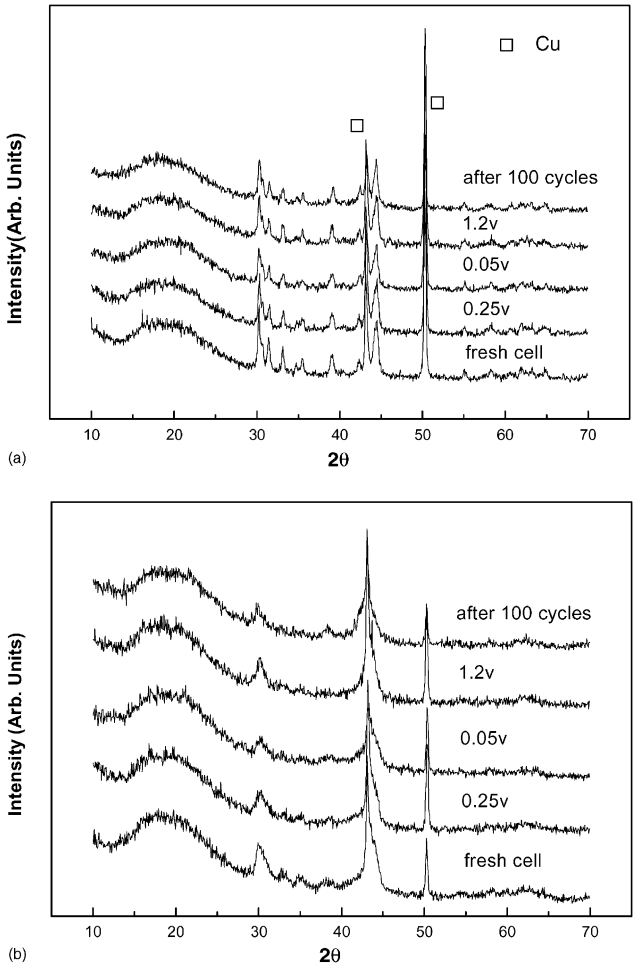

Fig. 5. Ex situ XRD patterns after first discharge and charge to a given voltage for sample milled for (a) 4 h and (b) 10 h. Note broad peak at low angle is due to scotch tape used for protection against air.

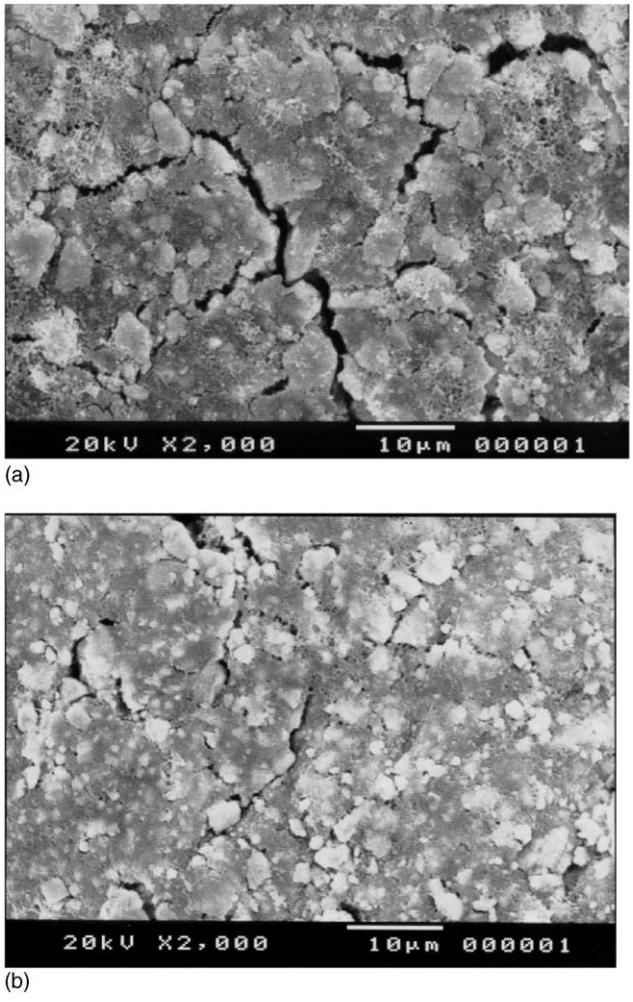

Fig. 6. Electron micrographs of electrodes after 100 cycles for samples subjected to ball milling for (a) 4 h and (b) 10 h.

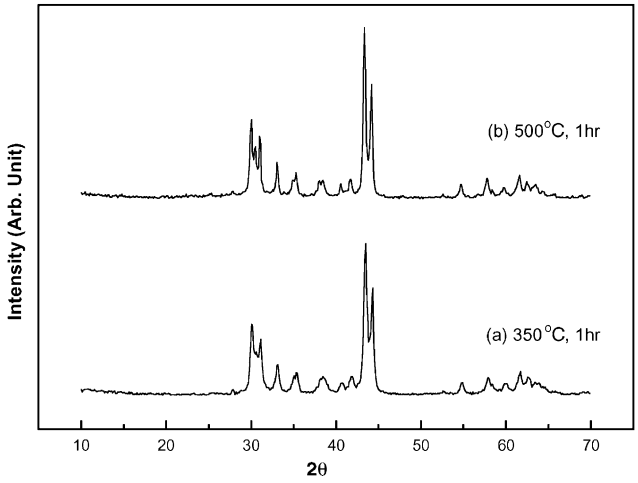

Fig. 7. XRD patterns after annealing 10 h ball-milled powders at (a) 350 °C and (b) 500 °C for 1 h in argon environment.

formation of a new phase even after 100 cycles (Fig. 5(a)). It seems, however, that when discharged to 0.05 V, a trace of a Li-rich phase is formed. This is indicated by a slight hump at $2\theta \approx 22^\circ$ and broadening of the Ni_3Sn_4 peak at 38°, i.e. peak positions which are related to Li–Sn alloy phases [9]. This can be also inferred from the occurrence of a peak near 0.7 V in the differential capacity curve of the first charge (Fig. 3(a)). This peak is attributable to Li-rich Li–Sn alloy phases [9], which disappear on extended cycling. The formation of these Li–Sn alloy phases is caused by the tin atoms which are unreacted during mechanical alloying for Ni_3Sn_4 formation, as presumed from the XRD pattern in Fig. 1 in which a trace of a pure-Ni peak is observed. In the case of the alloy milled for l0 h (Fig. 5(b)), the intensity of crystalline peaks slightly decreases but the main crystalline peaks at 30 and 43° are maintained during cycling. One apparent change in the XRD pattern is that broad peaks at approximately 22 and 38° are observed after 100 cycles and are related to Li–Sn alloy phases [9]. This reveals that some of the heavily strained, nanocrystalline phase decompose into inactive nickel and active tin. The formation of Li-rich alloy phases leads to fast mechanical degradation of the electrode due to a large volume change during cycling. This is supported by SEM of the electrodes which had failed mechanically after 100 cycles, as shown in Fig. 6.

At this point, it should be noted again that the Ni_3Sn_4 phase is maintained even after extended cycling. To obtain the well-developed nanocrystalline Ni_3Sn_4 phase, the sample milled for 10 h was heat-treated. The XRD patterns of the sample heat-treated at 350 and 500 °C for 1 h under argon flow are shown in Fig. 7(a) and (b), respectively. After heat-treatment, well-crystallized Ni_3Sn_4 phase is obtained. As the temperature is increased, the width of the diffraction peaks decreases, which indicates grain growth. The grain size of the samples heat-treated at 350 and 500 °C is estimated to be approximately 27 and 45 nm by XRD, respectively. Capacity versus cycle number plots for the heat-treated samples are given in Fig. 8. No capacity fading is observed. The capacity decreases with increase in the

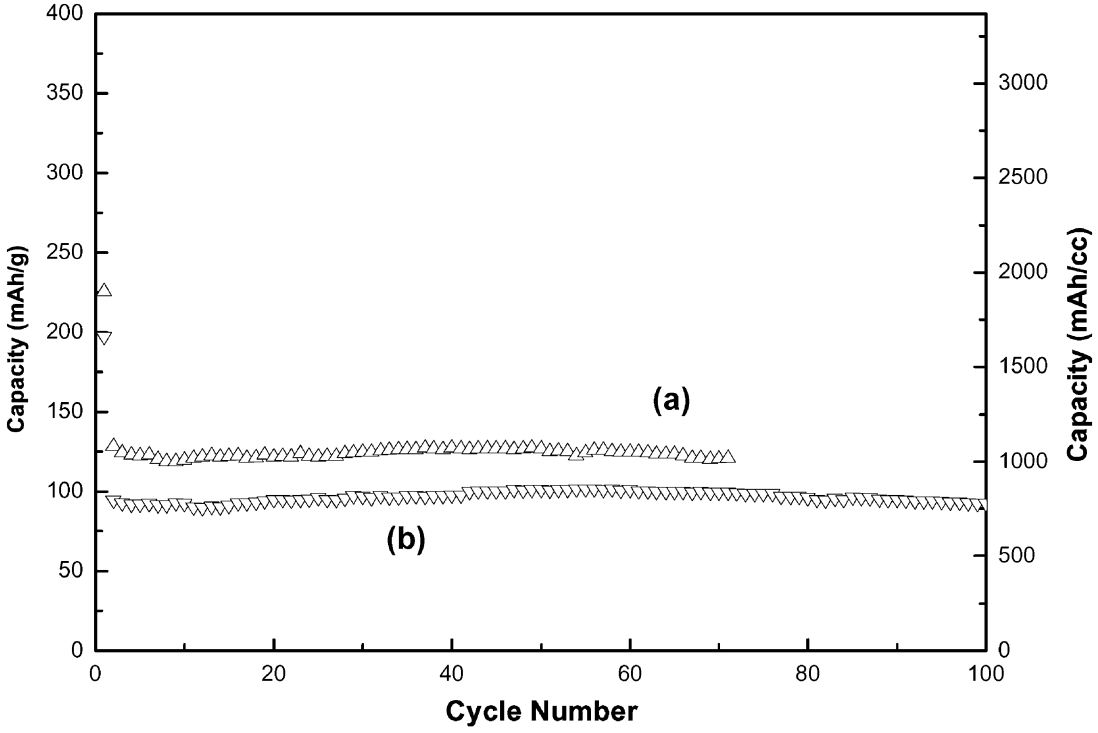

Fig. 8. Discharge capacity vs. cycle number for sample obtained by annealing at (a) 350 °C and (b) 500 °C.

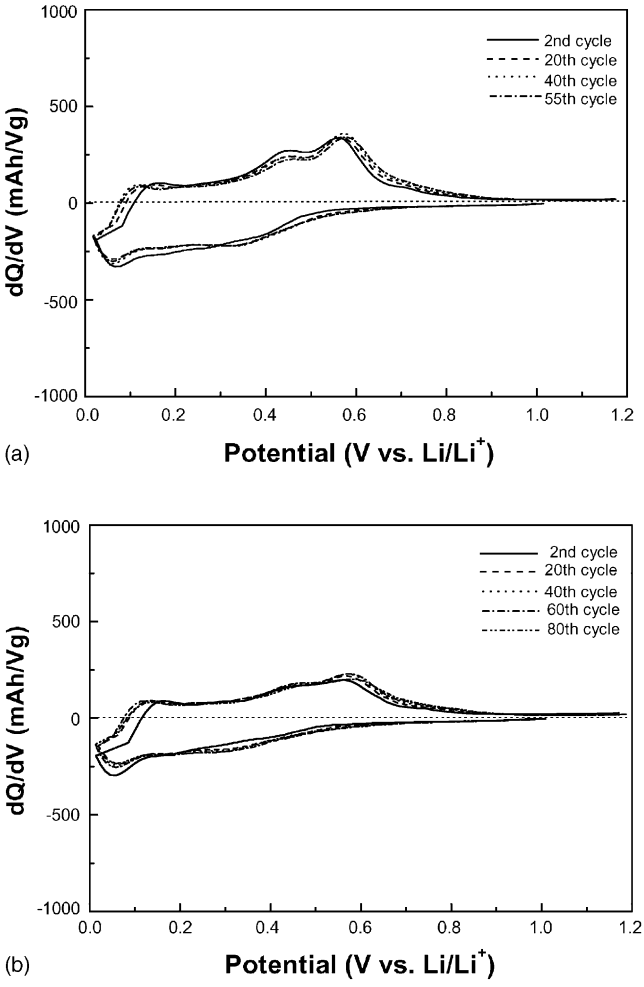

Fig. 9. Differential capacity vs. voltage for sample obtained by annealing at (a) 350 °C and (b) 500 °C.

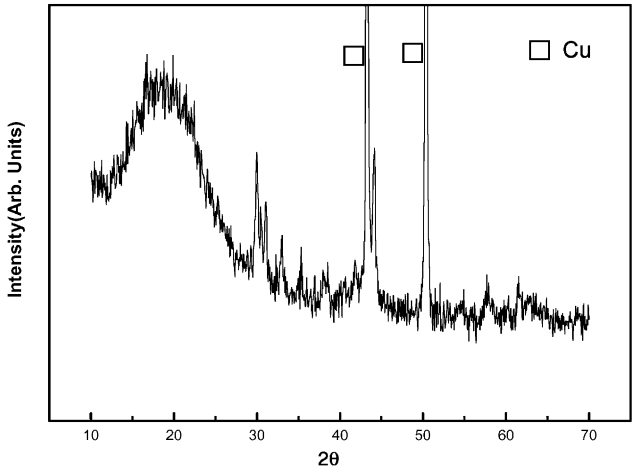

Fig. 10. Ex situ XRD pattern after subjecting sample annealed at 500 °C to 100 cycles.

heat-treatment temperature. The differential capacity versus voltage curves are very broad and unchanged for many charge–discharge cycles, as shown in Fig. 9. This suggests that the reaction mechanism is consistent and the active material is very stable for extended cycling. The XRD pattern of the alloy heat-treated at 500 °C after 100 cycles is given in Fig. 10. The crystallinity, including the peak positions and the full width at half maximum of the major diffraction peaks, is unchanged. An electron micrograph of the electrode after 100 cycles (not included here) also shows a smooth morphology with no cracking.

Based on these results, it can be concluded that lithium atoms react reversibly with tin atoms at and within the grain boundaries of Ni_3Sn_4, as found for nanostructured $SnMn_3C$ by Beaulieu et al. [8]. Correspondingly, the grain growth of crystalline Ni_3Sn_4 should reduce the capacity, as shown in Fig. 8, since the fraction of tin atoms decreases at the grain boundaries.

4. Conclusions

In this study, nanostructured samples of Ni_3Sn_4 have been examined as anodes for Li-ion batteries. It is found that lithium reacts reversibly with tin atoms in the grain boundaries of Ni_3Sn_4. The well-developed nanocrystalline Ni_3Sn_4 alloy demonstrates excellent cycle performance with no capacity fading.

Acknowledgements

This work was supported by The Korean Ministry of Science and Technology through the research programme of the National Research Laboratory.

References

[1] J. Yang, M. Winter, J.O. Besenhard, Solid State Ionics 90 (1996) 281.
[2] J.O. Besenhard, J. Yang, M. Winter, J. Power Sources 68 (1997) 87.
[3] R.A. Huggins, J. Power Sources 26 (1989) 109.
[4] O. Mao, J.R. Dahn, J. Electrochem. Soc. 146 (1999) 414.
[5] O. Mao, R.A. Dunlap, J.R. Dahn, J. Electrochem. Soc. 146 (1999) 405.
[6] K.D. Kepler, J.T. Vaughey, M.M. Thackeray, J. Power Sources 81–82 (1999) 383.
[7] G.X. Wang, L. Sun, D.H. Bradhurst, S.X. Dou, H.K. Liu, J. Alloys Compounds 299 (2000) L12.
[8] L.Y. Beaulieu, D. Larcher, R.A. Dunlap, J.R. Dahn, J. Electrochem. Soc. 147 (2000) 3206.
[9] I.A. Courtney, J.R. Dahn, J. Electrochem. Soc. 144 (1997) 2045.